
Conditional Diffusion Models for Uncertainty Estimation in Super Resolution Microscopy

Anonymous Author(s)

Affiliation

Address

email

Abstract

1 Deep learning has recently attracted considerable attention from researchers in
2 the natural sciences, particularly microscopists, for fast extraction of physically
3 relevant information from images. However, simple and interpretable uncertainty
4 quantification is lacking in these applications, and remains a necessary modeling
5 component in high-risk research. In order to quantify uncertainty in otherwise
6 deterministic image translation architectures, we propose a hybrid generative
7 modeling framework based on denoising diffusion probabilistic models (DDPMs).
8 Specifically, our model combines a deterministic neural network with a DDPM,
9 which can improve conditional synthesis speed and fidelity of the DDPM, while
10 providing a natural mechanism for uncertainty estimation via Langevin dynamics.
11 We apply our model to the task of single molecule localization in fluorescence
12 microscopy, and demonstrate that blending the DeepSTORM architecture with
13 a DDPM permits simultaneous high-fidelity super-resolution with uncertainty
14 estimation of kernel density estimates (KDEs) regressed by DeepSTORM. Our
15 results suggest the proposed solution is an interesting addition to the modeling
16 toolkit for fluorescence microscopists and the field of deep image translation in
17 general.

18 1 Introduction

19 Deep learning has attracted tremendous attention from researchers in the natural sciences, with
20 several foundational applications arising in microscopy, e.g., (Weigert 2018; Falk 2019). Recently,
21 the application of deep image translation in single-molecule localization microscopy (SMLM) has
22 received considerable interest (Ouyang 2018; Nehme 2020; Speiser 2021). SMLM techniques
23 are a mainstay of fluorescence microscopy and can be used to produce a pointillist representation
24 of biomolecules in the cell at diffraction-unlimited precision (Rust 2006; Betzig 2006). As this
25 technology enables increasingly precise measurements of the cellular environment, there is an
26 increasing need for machine learning methods to report uncertainty for quality control.

27 In previous applications of deep models to localization microscopy, super-resolution images can be
28 recovered from a sparse set of localizations with conditional generative adversarial networks (Ouyang
29 2018) or kernel density estimation can be performed using convolutional networks (Nehme 2020;
30 Speiser 2021). Here, we focus on the latter class of models which perform single molecule localization
31 using neural networks. In this approach, one estimates molecular coordinates by predicting kernel
32 density estimates (KDEs) y , which are latent in the raw data x , using a convolutional neural network.
33 Importantly, inferences in SMLM are often necessarily made on a single measurement, thus common
34 measures of model performance are based on localization errors computed over ensembles of
35 simulated images. However, this choice precludes computation of aleatoric uncertainty at test time
36 under a fixed model, and may result in the application of models to out of distribution datasets.



Figure 1: Generative model of single molecule localization microscopy images

Bayesian probability theory offers us mathematically grounded tools to reason about model uncertainty, but these usually come with a prohibitive computational cost (Gal 2022). A few approaches to avoiding this intractability in deep models have been deterministic uncertainty quantification (Amersfoort 2020), ensembling (Lakshminarayanan et al., 2017) or Monte Carlo dropout (Gal and Ghahramani, 2016). Here, we report a method which models estimates uncertainty in KDE predictions by combining deterministic deep learning with deep generative modeling in a hybrid algorithm. Our approach produces pixel-wise uncertainties in model predictions with no modification to the existing architecture, and can be used for downstream filtering of erroneous image regions. We choose to model a distribution on high-resolution KDE predictions conditioned on a low-resolution input using a denoising diffusion probabilistic model (DDPM) (Ho 2020; Song 2021), referred to here as simply “diffusion model”. Such models are one class of *score based generative models* which implicitly compute the score of the data distribution at each noise scale (Song 2021) and are well suited conditional image generation tasks (Saharia 2021). Most importantly, score-based models provide a natural mechanism for uncertainty quantification. Our approach could be readily integrated with existing localization performance measures to address both model accuracy on training data and precision on datasets produced by experiments.

2 Background

2.1 Image Likelihood and Localization Error

The central objective of single molecule localization microscopy is to infer a set of molecular coordinates θ from measured low resolution images \mathbf{x} . The likelihood on a particular pixel k , i.e., $p(\mathbf{x}_k|\theta)$ is taken to be a convolution of Poisson and Gaussian distributions, due to shot noise $p(s_k) = \text{Poisson}(\omega_k)$ and sensor readout noise $p(\zeta_k) = \mathcal{N}(o_k, \sigma_k^2)$

$$p(\mathbf{x}_k|\theta) = A \sum_{q=0}^{\infty} \frac{1}{q!} e^{-\omega_k} \omega_k^q \frac{1}{\sqrt{2\pi}\sigma_k} e^{-\frac{(\mathbf{x}_k - g_k q - o_k)^2}{2\sigma_k^2}} \approx \text{Poisson}(\omega'_k) \quad (1)$$

where A is some normalization constant and $\omega'_k = \omega_k + \sigma_k^2$. For the sake of generality, we include a per-pixel gain factor g_k , which is often unity. In practice, the summation in (1) can be difficult to work with, and it is common to instead use a Poisson-Normal approximation for simplification, valid under a range of experimental conditions (Huang 2013). This result can be seen from the fact the the convolution of two Poisson distributions is also Poisson. The expectation of the Poisson process at each pixel of the image is computed from the optical transfer function $O(u, v)$, which is often a two-dimensional isotropic Gaussian.

$$\omega = i_0 \int O(u) du \int O(v) dv \quad (2)$$

The above integration can be carried out by computing differences of error functions, as detailed in Appendix A. The complete generative process is depicted in Figure 1.

Reliable estimation of θ from \mathbf{x} , for example by maximum likelihood estimation or with a deep model, requires performance metrics for model selection. We use the Fisher information as an information theoretic criteria to assess the quality of the model tested here, with respect to the root mean squared error (RMSE) of our predictions of θ (Chao 2016). The Poisson log-likelihood $\ell(\mathbf{x}|\theta)$ is also convenient for computing the Fisher information matrix (Smith 2010) and thus the

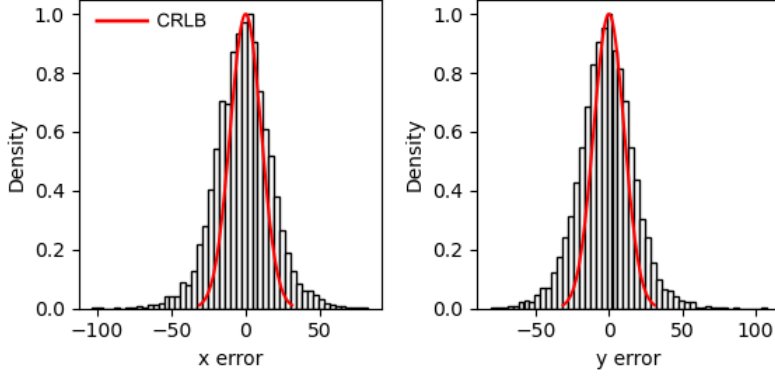


Figure 2: Localization errors of the trained model

73 Cramer-Rao lower bound, which bounds the variance of a statistical estimator of θ , from below
 74 i.e., $\text{var}(\hat{\theta}) \geq I^{-1}(\theta)$. The Fisher information is straightforward to compute under the Poisson
 75 log-likelihood, which is detailed in the Appendix

$$\mathcal{I}_{ij}(\theta) = \mathbb{E}_{\theta} \left(\frac{\partial \ell}{\partial \theta_i} \frac{\partial \ell}{\partial \theta_j} \right) = \sum_k \frac{1}{\omega'_k} \frac{\partial \omega'_k}{\partial \theta_i} \frac{\partial \omega'_k}{\partial \theta_j} \quad (3)$$

76 2.2 Kernel density estimation with deep networks

77 Direct optimization of the likelihood in (1) from observations \mathbf{x} alone is challenging when fluorescent
 78 emitters are dense within the field of view and fluorescent signals significantly overlap. However, con-
 79 volutional neural networks (CNN) have recently proven to be powerful tools fluorescence microscopy
 80 to extract parameters describing fluorescent emitters such as color, emitter orientation, z -coordinate,
 81 and background signal (Zhang 2018; Kim 2019; Zelger 2018). For localization tasks, CNNs typically
 82 employ upsampling layers to reconstruct Bernoulli probabilities of emitter occupancy (Speiser 2021)
 83 or kernel density estimates with higher resolution than experimental measurements (Nehme 2020).
 84 Kernel density estimates, denoted by \mathbf{y} , are the most common data structure used in SMLM, and can
 85 be easily generated from molecular coordinates, alongside observations \mathbf{x} , using well-understood
 86 models of the optical impulse response (Zhang 2007).

87 3 Conditional Diffusion for Uncertainty-Aware Super Resolution

88 We consider datasets $(\mathbf{x}_i, \mathbf{y}_i, \hat{\mathbf{y}}_i)_{i=1}^N$ of observed images \mathbf{x}_i true kernel density estimate (KDE) images
 89 \mathbf{y}_i , and KDE estimates $\hat{\mathbf{y}}_i = \phi(\mathbf{x}_i)$. Observations \mathbf{x}_i are simulated under the Poisson likelihood (1)
 90 and KDEs are generated using (2) alone, followed by appropriate normalization.

91 3.1 Problem Statement

92 Point estimates $\hat{\mathbf{y}}_i$ produced by the traditional deep architectures for super resolution microscopy
 93 produce strong results, but lack uncertainty quantification. Recent advances in generative modeling,
 94 particularly DDPMs, therefore present a unique opportunity to integrate uncertainty awareness into the
 95 super-resolution microscopy toolkit. However, sampling from DDPMs is computationally expensive,
 96 given that generation amounts to solving a complex stochastic differential equation, effectively
 97 mapping a simple base distribution to the complex data distribution. The solution of such equations
 98 requires numerical integration with very small step sizes, resulting in thousands of neural network
 99 evaluations (Saharia 2021; Vahdat 2021). Furthermore, for conditional generation tasks in high-risk
 100 applications, generation complexity is further exacerbated by the need for the highest level of detail
 101 in generated samples.

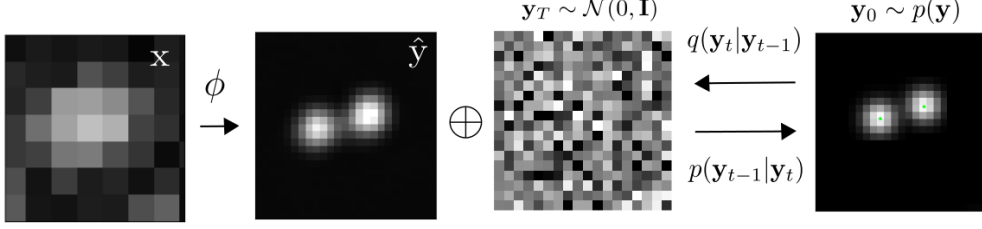


Figure 3: Conditional diffusion model for sampling kernel density estimates

Since we are primarily interested in the conditional distribution $p(\mathbf{y}|\mathbf{x})$, we propose that DDPM sampling is preceded by a deterministic transformation ϕ , trained to predict \mathbf{y} from \mathbf{x} . Reasoning for this choice in the current application is two-fold:

Synthesis Speed. By training a preprocessor ϕ to obtain an approximate estimate of \mathbf{y} , we can reduce the number of iterations, since the DDPM only needs to model the remaining mismatch, resulting in a less complex model from which sampling becomes easier. Speed is critical in SMLM applications, which can produce large volumes of image data in a single experiment. Moreover, we note that this approach is analogous to preconditioned stochastic gradient langevin dynamics (Li 2016), wherein ϕ identifies the posterior mode followed by Langevin dynamics to sample from the posterior.

Sample Fidelity. Since Langevin dynamics will often be initialized in low-density regions of the data distribution, inaccurate score estimation in these regions will negatively affect the sampling process (Song 2019). Moreover, mixing can be difficult because of the need of traversing low density regions to transition between modes of the distribution. Preprocessing with a deterministic mapping ϕ can ameliorate this issue, by eliminating the need for score estimation in low density regions.

The preprocessor ϕ is realized by a CNN with upsampling layers. Consider the Markov chain wherein the KDE \mathbf{y} is latent in and inferred from a noisy measurement \mathbf{x} , i.e., $\mathbf{x} \rightarrow \phi(\mathbf{x}) \rightarrow \hat{\mathbf{y}}$. By the data processing inequality the function ϕ can only destroy information in \mathbf{x} pertaining to \mathbf{y} i.e., $I(\mathbf{x}; \mathbf{y}) \geq I(\phi(\mathbf{x}); \mathbf{y})$ or $h(\mathbf{y}|\phi(\mathbf{x})) \geq h(\mathbf{y}|\mathbf{x})$ where I is the mutual information and h is the entropy. In other words, the function ϕ , while deterministic, can introduce additional uncertainty about \mathbf{y} in downstream stochastic models by destroying information. Here, we are interested in measuring the upper bound $h(\mathbf{y}|\phi(\mathbf{x}))$, as this is the relevant quantity when a deterministic transformation ϕ is an unavoidable first step.

In practice, a DDPM Ψ can be trained on pairs $(\mathbf{y}_i, \hat{\mathbf{y}}_i)_{i=1}^N$. The conditional DDPM generates a target KDE \mathbf{y}_0 in T refinement steps. Starting with a pure noise image $\mathbf{y}_T \sim \mathcal{N}(0, \mathbf{I})$, the model iteratively refines the KDE through successive iterations according to learned conditional transition distributions $p(\mathbf{y}_{t-1}|\mathbf{y}_t)$ such that $\mathbf{y}_0 \sim p(\mathbf{y}|\hat{\mathbf{y}})$

3.2 Uncertainty Estimation

Diffusion models (Sohl-Dickstein 2015; Ho 2020) are a class of generative models inspired by nonequilibrium statistical physics, which slowly destroy structure in a data distribution $p(\mathbf{y}_0|\mathbf{x})$ via a fixed Markov chain referred to as the *forward process*. In the present context, we apply leverage recent results from (Ho 2020; Song 2021; Saharia 2021) for applying this framework to sampling from $p(\mathbf{y}|\mathbf{x}, \hat{\mathbf{y}})$. We note that this approach is analogous to preconditioned stochastic gradient langevin dynamics (Li 2016), wherein ϕ identifies the posterior mode followed by sampling with Langevin dynamics. The forward process gradually adds Gaussian noise to the KDE \mathbf{y} according to a variance schedule $\beta_{0:T}$

$$q(\mathbf{y}_t|\mathbf{y}_0) = \prod_{t=1}^T q(\mathbf{y}_t|\mathbf{y}_{t-1}) \quad q(\mathbf{y}_t|\mathbf{y}_{t-1}) = \mathcal{N}\left(\sqrt{1-\beta_t}\mathbf{y}_{t-1}, \beta_t\mathbf{I}\right) \quad (4)$$

The usual procedure is then to learn a parametric representation of the *reverse process*, and therefore generate samples from $p(\mathbf{y}_0)$, starting from noise. Formally, $p_\theta(\mathbf{y}_0|\hat{\mathbf{y}}) = \int p_\theta(\mathbf{y}_{0:T}|\hat{\mathbf{y}})d\hat{\mathbf{y}}_{1:T}$ where

140 \mathbf{y}_t is a latent representation with the same dimensionality of the data. $p_\theta(\mathbf{y}_{0:T}|\hat{\mathbf{y}})$ is a Markov process,
 141 starting from a noise sample $p_\theta(\mathbf{y}_T) = \mathcal{N}(0, \mathbf{I})$.

$$p_\theta(\mathbf{y}_{0:T}) = p_\theta(\mathbf{y}_T) \prod_{t=1}^T p_\theta(\mathbf{y}_{t-1}|\mathbf{y}_t) \quad p_\theta(\mathbf{y}_{t-1}|\mathbf{y}_t) = \mathcal{N}(s_\theta(\mathbf{y}_t), \beta_t I) \quad (5)$$

142 where we reuse the variance schedule of the forward process (Ho 2020). We omit conditioning
 143 on $\hat{\mathbf{y}}$ for each transition density $p_\theta(\mathbf{y}_{t-1}|\mathbf{y}_t)$, as this is only considered at $t = 0$ i.e., $p_\theta(\mathbf{y}_1|\mathbf{y}_0, \hat{\mathbf{y}})$.
 144 An important property of the forward process is that it admits sampling \mathbf{y}_t at an arbitrary timestep
 145 t in closed form (Ho 2020). Using the notation $\alpha_t := 1 - \beta_t$ and $\gamma_t := \prod_{s=1}^t \alpha_s$, we have
 146 $q(\mathbf{y}_t|\mathbf{y}_0) = \mathcal{N}(\sqrt{\gamma_t}\mathbf{y}_0, (1 - \gamma_t)I)$. Training is performed by optimizing the usual variational bound
 147 on negative log likelihood:

$$\mathcal{L}(\theta) = \mathbb{E}[-\log p_\theta(\mathbf{y}_0|\mathbf{x})] \leq \mathbb{E}\left[-\log \frac{p_\theta(\mathbf{y}_{0:T}|\mathbf{x})}{q(\mathbf{y}_{1:T}|\mathbf{y}_0)}\right] \quad (6)$$

148 The objective in (6) can be expanded in terms of $D_{\text{KL}}(p(\mathbf{y}_{t-1}|\mathbf{y}_t)||q(\mathbf{y}_t|\mathbf{y}_{t-1}))$ as detailed in (Ho
 149 2020). We choose to adopt the simplified form of the variational bound, which emphasizes that the
 150 DDPM estimates the score $\nabla_{\mathbf{y}} \log p(\mathbf{y}|\mathbf{x})$ at each noise level (Song 2021)

$$\theta^* = \underset{\theta}{\operatorname{argmin}} \mathbb{E}_{(\hat{\mathbf{y}}, \mathbf{y}_0) \sim (\epsilon, \gamma)} \mathbb{E} \left[s_\theta \left(x, \sqrt{\gamma}\mathbf{y}_0 + \sqrt{1 - \gamma}\epsilon \middle| \mathbf{y}_t, \gamma \right) - \epsilon \right], \quad (7)$$

151 After training, samples can be generated by

$$\mathbf{y}_{t-1} = \frac{1}{\sqrt{1 - \beta_t}} (\mathbf{y}_t + \beta_t s_\theta(\mathbf{y}_t)) + \sqrt{\beta_t} \xi \quad (8)$$

152 The distribution of γ has a big impact on the quality of the model and the generated outputs. For our
 153 training noise schedule, we use a piecewise distribution for γ , $p(\gamma) = \frac{1}{T} \sum_{t=1}^T U(\gamma_{t-1}, \gamma_t)$ (Nanxin
 154 2021). Specifically, during training, we first uniformly sample a time step $t \sim \{0, \dots, T\}$ followed by
 155 sampling $\gamma \sim U(\gamma_{t-1}, \gamma_t)$.

156 4 Experiments

157 All training data consists of low-resolution 20×20 images, simulated under the likelihood and impulse
 158 response (2,10), and KDEs with dimension 80×80 scaled between $[0, 1]$. For a typical CMOS camera,
 159 this results in KDE pixels with lateral dimension of $\approx 27\text{nm}$. Initial coordinates θ were drawn
 160 uniformly over a disc with a radius of 7 low-resolution pixels.

161 4.1 Model Precision on Simulated Ensembles

162 4.2 Model Uncertainty

163 We set $T = 100$ for all experiments and treat forward process variances β_t as hyperparameters,
 164 with a linear schedule from $\beta_0 = 10^{-4}$ to $\beta_T = 10^{-2}$. These constants were chosen to be small
 165 relative to ground truth KDEs, which are scaled to $[-1, 1]$, ensuring that forward process distribution
 166 $\mathbf{y}_T \sim q(\mathbf{y}_T|\mathbf{y}_0)$ approximately matches the reverse process $\mathbf{y}_T \sim \mathcal{N}(0, I)$ at $t = T$.

167 To represent the reverse process, we used a DDPM architecture based on a U-Net backbone proposed
 168 in (Saharia 2021). We chose a U-Net backbone with channel multipliers $[1, 2, 4, 8, 8]$ in the downsam-
 169 pling and upsampling paths of the architecture. Parameters are shared across time, which is specified
 170 to the network using the Transformer sinusoidal position embedding. We use self-attention at the
 171 16×16 feature map resolution. To condition the model on the input $\hat{\mathbf{y}}$, we concatenate the $\hat{\mathbf{y}}$ estimated
 172 by DeepSTORM along the channel dimension, which are scaled to $[0, 1]$, with $\mathbf{y}_T \sim \mathcal{N}(0, I)$. Others
 173 have experimented with more sophisticated methods of conditioning, but found that the simple
 174 concatenation yielded similar generation quality (Saharia 2021).

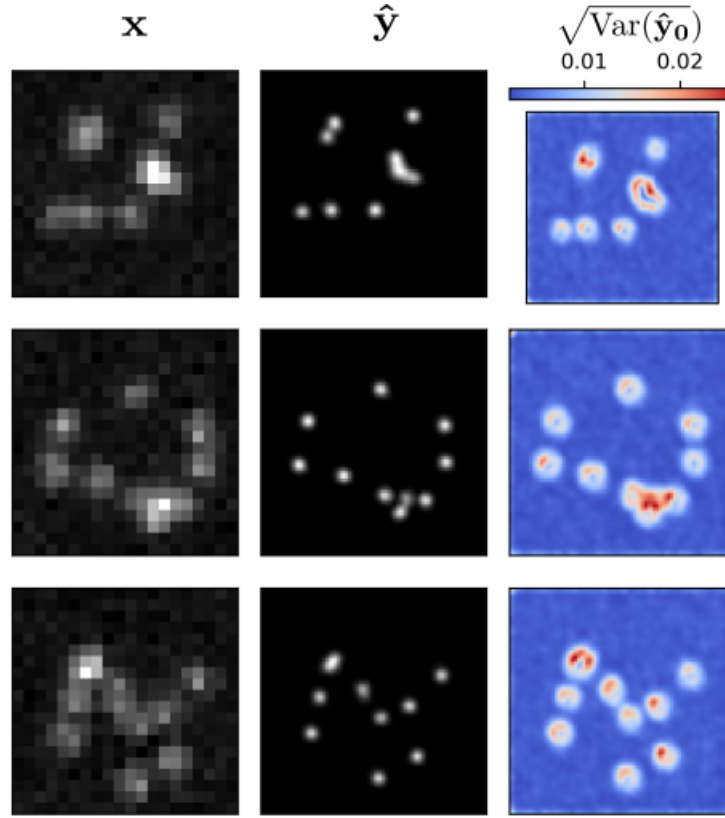


Figure 4: Kernel density estimates for various signal to noise ratios (SNR)

5 Related Work

6 Conclusion

References

- [1] Nehme, E., et al. *DeepSTORM3D: dense 3D localization microscopy and PSF design by deep learning*. Nature Methods 17, 734–740 (2020).
- [2] Ouyang, W., et al. *Deep learning massively accelerates super-resolution localization microscopy*. Nature Biotechnology 36, 460–468 (2018).
- [3] Speiser, A., et al. *Deep learning enables fast and dense single-molecule localization with high accuracy*. Nature Methods 18, 1082–1090 (2021).
- [4] Sohl-Dickstein J., et al. *Deep unsupervised learning using nonequilibrium thermodynamics*. ICLR (2015).
- [5] Ho J., et al. *Denoising Diffusion Probabilistic Models*. Advances in Neural Information Processing Systems (2015).
- [6] Nanxin C., et al. *WaveGrad: Estimating Gradients for Waveform Generation*. ICLR (2021).
- [4] Chao, J., et al. *Fisher information theory for parameter estimation in single molecule microscopy: tutorial*. Journal of the Optical Society of America A 33, B36 (2016).
- [5] Schermelleh, L. et al. *Super-resolution microscopy demystified*. Nature Cell Biology vol. 21 72–84 (2019).
- [6] Zhang, B., et al. *Gaussian approximations of fluorescence microscope point-spread function models*. (2007).
- [7] Smith, C.S., *Fast, single-molecule localization that achieves theoretically minimum uncertainty*. Nature Methods 7, 373–375 (2010).

- 194 [8] Nieuwenhuizen, R., et al. *Measuring image resolution in optical nanoscopy*. Nature Methods 10, 557-562
195 (2013).
- 196 [9] Huang, F., et al. *Video-rate nanoscopy using sCMOS camera-specific single-molecule localization algorithms*.
197 Nat Methods 10, 653–658 (2013).
- 198 [10] Rust, M., et al. *Sub-diffraction-limit imaging by stochastic optical reconstruction microscopy (STORM)*.
199 Nat Methods 3, 793–796 (2006).
- 200 [11] Betzig, E., et al. *Imaging intracellular fluorescent proteins at nanometer resolution*. Science 313, 1642–1645
201 (2006).
- 202 [12] Weigert, M., et al. *Content-aware image restoration: pushing the limits of fluorescence microscopy*. Nat.
203 Methods 15, 1090 (2018).
- 204 [13] Falk, T., et al. *U-net: deep learning for cell counting, detection, and morphometry*. Nat. Methods 16, 67–70
205 (2019).
- 206 [14] Boyd, N., et al. *DeepLoco: fast 3D localization microscopy using neural networks*. Preprint at bioRxiv
207 <https://doi.org/10.1101/267096> (2018)
- 208 [15] Zelger, P., et al. *Three-dimensional localization microscopy using deep learning*. Opt. Express 26,
209 33166–33179 (2018)
- 210 [16] Zhang, P., et al. *Analyzing complex single-molecule emission patterns with deep learning*. Nat. Methods 15,
211 913 (2018)
- 212 [17] Saharia, C., et al. *Image Super-Resolution via Iterative Refinement*. Preprint at arXiv
213 <https://doi.org/10.48550/arXiv.2104.07636> (2021)
- 214 [18] Kim, T., et al. *Information-rich localization microscopy through machine learning*. Nat Commun 10, 1996
215 (2019).

216 A Appendix

217 Standard SMLM localization algorithms based on maximum likelihood estimators or least squares
218 optimization require tight control of activation and reactivation to maintain sparse emitters, presenting
219 a tradeoff between imaging speed and labeling density. Recently, deep models have generalized
220 SMLM to densely labeled structures by predicting high-resolution kernel density estimates (KDEs)
221 from low resolution images with convolutional networks. However, estimated KDEs may contain
222 irregularities due to finite sample sizes and limited model capacity.

223 The DeepSTORM CNN, initially proposed in (Nehme 2020) for 3D localization, can be viewed
224 as a deep kernel density estimator, reconstructing kernel density estimates \mathbf{y} from low-resolution
225 inputs \mathbf{x} . We utilize a simplified form of the original architecture for 2D localization, which we
226 denote ϕ hereafter, which consists of three main modules: a multi-scale context aggregation module,
227 an upsampling module, and a prediction module. For context aggregation, the architecture utilizes
228 dilated convolutions to increase the receptive field of each layer. The upsampling module is then
229 composed of two consecutive 2x resize-convolutions, computed by nearest-neighbor interpolation,
230 to increase the lateral resolution by a factor of 4. For a common sCMOS camera, each pixel has a
231 lateral size of approximately 108 nanometers, giving approximately 27 nanometer pixels in the KDE.
232 The terminal prediction module contains three additional convolutional blocks for refinement of the
233 upsampled image, followed by an element-wise HardTanh.

234 Single molecule localization microscopy (SMLM) relies on the temporal resolution of fluorophores
235 whose spatially overlapping point spread functions would otherwise render them unresolvable
236 at the detector. Common strategies for the temporal separation of molecules involve molecular
237 photoswitching from dark to fluorescent states, permitting resolution of fluorophores beyond the
238 diffraction limit. Estimation of molecular coordinates is typically carried out by modeling the optical
239 impulse response of the imaging system and fitting model functions to the data. However, such
240 models are only well-suited to isolated molecules, reducing the number of molecules in the field of
241 view and limiting temporal resolution in super resolution microscopy. This issue has incited a series
242 of efforts to increase the density of fluorescent molecules imaged in a single frame while developing
243 appropriate models for dense localization.

244 In fluorescence microscopy, each pixel is treated as a Poisson random variable (Smith 2010; Nehme
245 2020; Chao 2016), with expected value

$$\omega = i_0 \int O(u)du \int O(v)dv \quad (9)$$

where $i_0 = \eta N_0 \Delta$. The scalar parameters η, Δ are the photon detection probability of the sensor and the exposure time, respectively. Without loss of generality, we assume $\eta = \Delta = 1$. Most importantly, N_0 represents the signal amplitude, which we assume maintains a fixed value. The optical impulse response $O(u, v)$ is often approximated as a 2D isotropic Gaussian with standard deviation σ (Zhang 2007). This approximation has the convenient property, that the effects of pixelation can be expressed in terms of error functions. For example, given a fluorescent emitter located at $\theta = (u_0, v_0)$, we have that

$$\int O(u)du = \frac{1}{2} \left(\operatorname{erf} \left(\frac{u_k + \frac{1}{2} - u_0}{\sqrt{2}\sigma} \right) - \operatorname{erf} \left(\frac{u_k - \frac{1}{2} - u_0}{\sqrt{2}\sigma} \right) \right) \quad (10)$$

where we have used the common definition $\operatorname{erf}(z) = \frac{2}{\sqrt{\pi}} \int_0^t e^{-t^2} dt$. Our generative model also incorporates a normally distributed white noise per pixel ζ with offset o and variance σ^2 . Ultimately, we have a Poisson component of the signal, which scales with N_0 and a Gaussian component, which does not.

Consider,

$$\zeta_k - o_k + \sigma_k^2 \sim \mathcal{N}(\sigma_k^2, \sigma_k^2) \approx \text{Poisson}(\sigma_k^2) \quad (11)$$

Since $\mathbf{x}_k = \mathbf{s}_k + \zeta_k$, we transform $\mathbf{x}'_k = \mathbf{x}_k - o_k + \sigma_k^2$, which is distributed according to

Consider the factorization $p(\hat{\mathbf{y}}|\mathbf{x}, \mathbf{y})p(\mathbf{x}|\mathbf{y})p(\mathbf{y}) = p(\mathbf{x}|\mathbf{y}, \hat{\mathbf{y}})p(\mathbf{y}|\hat{\mathbf{y}})p(\hat{\mathbf{y}})$. Given that \mathbf{x} is conditionally independent of $\hat{\mathbf{y}}$, we find

$$p_{\Psi}(\hat{\mathbf{y}}|\mathbf{x}, \mathbf{y}) = p(\mathbf{y}|\hat{\mathbf{y}})$$